Original
ISSN 2413-0516

The Protective Effect of 3-O-Acetyl-11-Keto-Beta Boswellic Acid-Nanostructured Lipid Carriers and Magnesium Oxide Nanoparticles on Experimental Liver Fibrosis

Afraa Alsamkari[1*], Gamal Said Abd El-Aziz[2], Emad Ahmed Hindi[2], Osama Abdelhakim Aly Ahmed[3]

[1]Department of Anatomy, Faculty of Medicine in Rabigh, King Abdulaziz University, Rabigh 25732, Saudi Arabia.
[2]Department of Clinical Anatomy, Faculty of Medicine, King Abdulaziz University, Jeddah 21589, Saudi Arabia.
[3]Department of Pharmaceuticals, Faculty of Pharmacy, King Abdulaziz University, Jeddah 21589, Saudi Arabia.
*Correspondence to: Afraa Alsamkari (E-mail: fwlsamkari@kau.edu.sa)
(Submitted: 22 March 2025 – Revised version received: 04 April 2025 – Accepted: 03 May 2025 – Published online: 26 June 2025)

Abstract

Objective: Chronic liver disease is a global burden, causing 2 million deaths annually. No FDA-approved treatment exists. This study aimed to compare 3-acetyl-11-keto-beta-boswellic acid (AKBA), magnesium oxide nanoparticles (MgO NPs), and AKBA-nanostructured lipid carriers (AKBA-NLCs) combined with MgO NPs (AKBA-NLCs + MgO NPs) in the treatment of thioacetamide (TAA)-induced liver fibrosis in rats.

Methods: AKBA-NLCs were prepared using high-shear homogenization, emulsification, and sonication, and characterized using DLS and TEM. Twenty-five Wistar male rats (N = 25) were randomly assigned to five groups; Group 1 (normal control group) received 1 ml of distilled water via i.p. (intraperitoneal), thrice weekly for 4 weeks, and 1 ml p.o. (by oral gavage). Group 2 (TAA group) received TAA (200 mg/kg body weight (b.wt.), i.p.), 3 times weekly for 4 weeks. Group 3 (TAA + MgO NPs group) received TAA and MgO NPs (100 µg/ml, p.o.). Group 4 (TAA + AKBA group) received TAA and AKBA (10 mg/kg b.wt., p.o.). Group 5 (TAA + AKBA-NLCs + MgO NPs group) received AKBA-NLCs and MgO NPs (10 mg/kg b.wt. + 100 µg/mL, p.o.). All groups, except Group 1, received the same thioacetamide dosage as Group 2. All groups, except group 2, received their oral treatments/ vehicle daily for 4 weeks. Liver injury was assessed via serum biomarkers (ALT, AST, albumin, and total bilirubin), cytokines (TNF-α, IL-1β, IL-6, and GSH), and staining with hematoxylin and eosin (H&E), Masson's Trichrome, and α-smooth muscle actin (α-SMA) immunohistochemistry. One-way analysis of variance (ANOVA) and Tukey–Kramer tests were used for analyzing data, and $P < 0.05$ was considered statistically significant.

Results: Liver serology, inflammatory, and oxidative stress markers were comparably reduced in all treatment groups; however, collagen deposition and α-SMA expression were significantly lower in the combination group.

Conclusion: This dual nanomedicine approach warrants further investigation as a therapeutic strategy.

Keywords: Liver fibrosis, AKBA, magnesium oxide nanoparticles, nanostructured lipid carriers, thioacetamide

Introduction

Chronic liver disease is an emergent medical concern with a massive burden globally.[1] Every year, approximately two million deaths occur due to chronic liver disease and cirrhosis.[2] Chronic liver disease culminates in liver fibrosis. Eventually, liver fibrosis leads to cirrhosis and subsequently to hepatocellular carcinoma. Alcohol-related liver disease, metabolic-associated liver disease, chronic viral hepatitis, and autoimmune hepatitis are chronic liver diseases, and they lead to hepatic fibrosis. In response to chronic liver injury, a healing scar consisting of collagen fibers laid by hepatic stellate cells replaces hepatocytes and leads to liver fibrosis.[3] Liver transplantation is the only treatment. Liver fibrosis is a reversible stage.[4] However, an FDA-approved treatment is still lacking while liver fibrosis is on the rise.[5]

The use of nanomaterials, including both natural and synthetic types, represents a promising direction in the management of liver fibrosis.[6] Magnesium oxide nanoparticles (MgO NPs) are renowned for their potent antioxidant properties.[7] Oxidative stress is the primary mechanism by which liver fibrosis is initiated and propagated in many disease models, including the thioacetamide (TAA)-induced animal model.[8] Additionally, MgO NPs have shown efficacy in alleviating cardiotoxicity induced by the DNA-intercalating drug doxorubicin.[9] This cardioprotective effect, mediated through antioxidative and anti-apoptotic pathways, reinforces the systemic protective role of MgO NPs against chemically induced organ damage, which parallels the hepatotoxic context of thioacetamide-induced fibrosis.

Boswellia species plants grow in India, China, and Arab countries, and they have been used as traditional therapies. The 3-acetyl-11-keto-beta-boswellic acid (AKBA) is a pentacyclic triterpenoid obtained from Boswellia serrata. AKBA is renowned for suppressing inflammation in various disease conditions, including osteoarthritis, rheumatoid arthritis, and inflammatory bowel disease.[10] In a rat model of high-fructose diet-induced nonalcoholic fatty liver disease (NAFLD), AKBA significantly reduced tumor necrosis factor-alpha (TNF-α) and interleukin-6 (IL-6) after only 6 weeks of administration.[11] It targets 5-lipoxygenase (5-LO), an enzyme involved in the metabolism of arachidonic acid to leukotrienes, which drive chemotaxis, vascular permeability, and immune cell activation during liver inflammation. In the liver, 5-LO activates hepatic stellate cells, which are major contributors to fibrosis.[12] AKBA also inhibits cyclooxygenase-2 (COX-2) and suppresses the nuclear factor-kappa B (NF-κB) pathway by stabilizing its inhibitor kappa B alpha (IκBα) and thus decreasing the expression of the inflammatory cascade, including TNF-α, IL-6, and interleukin-1β.[13] Although AKBA showed anti-inflammatory,

antioxidant, and anti-cancer properties in the literature, its effectiveness is hindered by poor water solubility and oral bioavailability.[14] Therefore, investigators are attempting to enhance the absorption of boswellic acid derivatives by several methods, including nanoformulations.[15–18]

Nanostructured lipid carriers (NLCs) are drug delivery systems known for their imperfect crystalline matrix structure, which enhances the bioavailability of drugs.[19] The core matrix of NLCs is composed of both solid and liquid lipids.[20] Nanoparticles are defined by a size range of 0–100 nm, though this definition is often extended to include particles up to 500 nm.[21] As noted in the review by Goel *et al.*, numerous nano-herbal formulations were tested for liver treatment, such as silybin nanoemulsion and naringenin nanoparticles.[20] NLCs enhance drug delivery by being absorbed through intestinal M cells directly into the lymphatic system, thereby avoiding extensive hepatic metabolism.[22] Nanoparticles are also engulfed by liver macrophages, which is expected to further enhance drug delivery.[23]

To date, no previous studies have investigated the effectiveness of MgO NPs, AKBA, or AKBA-NLCs combined with MgO NPs (AKBA-NLCs + MgO NPs) in the treatment of liver fibrosis in a rat model induced by TAA. This study aims to investigate and compare the therapeutic efficacy of MgO NPs, AKBA, and AKBA-NLCs + MgO NPs in the TAA-injected Wistar rat model of liver fibrosis in terms of their effects on oxidative stress, inflammatory cytokines, α-SMA immunohistochemical expression of activated hepatic stellate cells, and collagen production.

Materials and Methods

Chemicals and Reagents

All chemicals and reagents used in this study were of analytical grade and were purchased from reputable suppliers. 3-acetyl-11-keto-beta-boswellic acid (AKBA; CAS No. 67416-61-9) was obtained from Alfa Chemistry (Holbrook, NY, USA). Magnesium oxide nanoparticles (MgO NPs; CAT No. 549649), thioacetamide (TAA; CAT No. 163678), 1-Oleoyl-rac-glycerol (CAT No. M7765), Poloxamer 407 (CAT No. 16758), and other excipients were purchased from Sigma-Aldrich (St. Louis, MO, USA). Precirol ATO 5 (CAT No. 3092) was obtained from Gattefossé (La Défense, France). Goat Anti-Rabbit IgG H&L (HRP) (AB6721), Anti-α smooth muscle actin antibody (AB24964), and DAB Substrate Kit (AB64238) were procured from Abcam (Cambridge, UK).

Preparation of AKBA-Loaded Nanostructured Lipid Carriers (AKBA-NLCs)

AKBA-NLCs were formulated using a modified high-shear homogenization and ultrasonication technique as described by Ajiboye *et al.*[24] Briefly, the lipid phase, comprising 750 mg of Precirol ATO 5 and 250 mg of 1-Oleoyl-rac-glycerol, was heated to 70°C to ensure complete melting. AKBA (125 mg) was dissolved in the molten lipid phase. The aqueous phase, containing 500 mg of Poloxamer 407 as a surfactant, was heated to 70°C and gradually added to the lipid phase under magnetic stirring. The resulting pre-emulsion was immediately transferred to a high-shear mixer homogenizer (Ultra-Turrax® IKA T 25 D Basic, Staufen, Germany) and homogenized at 20,000 rpm for 7 minutes. The nanoemulsion was then transferred to a bath sonicator (UltraWave QS10 Ultrasonic Cleaner, South Korea) and sonicated for another 7 minutes. The final formulation was cooled to room temperature for 4 hours to allow lipid matrix solidification and then stored at 4°C.

Characterization of AKBA-NLCs

Dynamic light scattering (DLS) analysis was performed using a Malvern Zetasizer (Nano ZSP, Malvern Instruments, UK) to estimate the mean particle size (Z-average), polydispersity index (PDI), and zeta potential of the AKBA-NLCs. Samples were appropriately diluted with distilled water. Measurements were taken at a backscattering angle of 173 degrees and a temperature of 25°C. This method was adapted from Ajiboye *et al.*[24]

Transmission Electron Microscopy (TEM)

Transmission electron microscopy (JEM-100 CXII, JEOL Ltd., Japan), operated at 80 kV, was used to measure the particle size of the AKBA-NLCs. A well-dispersed AKBA-NLCs sample was placed on a carbon-coated copper grid mesh and stained with 2% (w/v) phosphotungstic acid solution. Excess stain was removed using filter paper, and the grid was left to air-dry for 10 minutes before analysis.[16]

Animal Model and Experimental Design

Twenty-five male Wistar rats, weighing 200–250 g, were obtained from King Fahd Medical Research Center (KFMRC), King Abdulaziz University (Jeddah, Saudi Arabia). Rats were housed at KFMRC under standard laboratory conditions. Environmental parameters were maintained at 25 ± 2°C temperature, 50% humidity, and 12-hour light/dark cycles. Rats had free access to food and water throughout the experimental period, including a one-week acclimatization period.

All experimental procedures were approved by the Animal Care and Use Committee (ACUC) of King Abdulaziz University (Approval No. ACUC-24-10-21). All animal protocols complied with the guidelines of the National Institutes of Health Guide for the Care and Use of Laboratory Animals (NIH Publication No. 8023, revised 1978).

Rats were randomly assigned to five groups, each consisting of five rats (n = 5). Group 1 served as the normal control group and received 1 mL of distilled water intraperitoneally (i.p.) three times per week for 4 weeks, followed by 1 mL orally (p.o.) daily for 4 weeks. Group 2 (TAA group) received thioacetamide (TAA; 200 mg/kg b.wt., i.p.) three times per week for 4 weeks. Group 3 (TAA + MgO NPs group) received MgO NPs (100 µg/mL, p.o.) daily for 4 weeks. Group 4 (TAA + AKBA group) received AKBA (10 mg/kg b.wt., p.o.) daily for 4 weeks. Group 5 (TAA + AKBA-NLCs + MgO NPs group) received AKBA-NLCs combined with MgO NPs (10 mg/kg b.wt. + 100 µg/mL, p.o.) daily for 4 weeks.

All groups, except Group 1, received the same TAA dosage as Group 2. The selected dosage and treatment duration for TAA were based on the study by Alkreathy and Esmat *et al.*[25] The MgO NPs dosage was adapted from Mazaheri *et al.*,[26] and the AKBA dosage was derived from the study by Khan *et al.*[18]

TAA was freshly dissolved in sterile distilled water before each administration to ensure stability. MgO NPs were suspended in distilled water and subjected to brief sonication to achieve uniform dispersion before oral gavage.

Twenty-four hours after the completion of the experiment, rats were anesthetized using isoflurane, and blood samples were collected via cardiac puncture. Blood was centrifuged at 4000 rpm for 15 minutes and stored at −80°C.[27] Animals were euthanized by cervical dislocation, and livers were harvested for homogenate preparation and histological assessment. Hepatic tissue intended for homogenate testing was stored at −80°C.[28]

Ethical Approval

All animal procedures were approved by the Animal Care and Use Committee (ACUC) of King Abdulaziz University, Jeddah, Saudi Arabia (Approval No. ACUC-24-10-21). All experiments were conducted in strict accordance with the guidelines of the National Institutes of Health Guide for the Care and Use of Laboratory Animals (NIH Publication No. 8023, revised 1978), and all efforts were made to minimize animal suffering.

Biochemical Assessments

Colorimetric enzyme-linked immunosorbent assay (ELISA) kits were provided by MyBioSource (San Diego, CA, USA) for biochemical analysis. The following kits were used to assess liver homogenate pro-inflammatory cytokines and oxidative status: Rat Tumor Necrosis Factor-α (TNF-α; CAT No. MBS8579427), Rat Interleukin-1β (IL-1β; CAT No. MBS265868), Rat Interleukin-6 (IL-6; CAT No. MBS269892), and reduced glutathione (GSH; CAT No. MBS265966).

Serum levels of liver function markers, including alanine aminotransferase (ALT; CAT No. MBS269614), aspartate aminotransferase (AST; CAT No. MBS264975), albumin (CAT No. MBS2022813), and total bilirubin (CAT No. MBS730053), were measured according to the manufacturer's instructions.

Histopathological Examination

After fixation of liver sections in 10% neutral-buffered formalin, tissue processing and paraffin embedding were performed. Liver histological sections (4 µm) were stained with hematoxylin and eosin (H&E) and Masson's Trichrome for collagen deposition according to established protocols.[29] Slides were visualized using light microscopy (Olympus BX53, Tokyo, Japan), and microphotographs were taken with the DP72 imaging system (Evident Corporation, Tokyo, Japan).

Fibrosis staging was performed using the METAVIR scoring system by a blinded histopathologist.[30] Blue-stained collagen fibers were quantified as fibrosis area percent. Quantification was conducted using image analysis software (ImageJ 1.52p, NIH, Bethesda, MD, USA). For each group, at least five random fields from representative slides were imaged at ×100 magnification, saved as TIF images, color deconvoluted, and thresholded to isolate either Masson's Trichrome (MT)-stained collagen or DAB-positive areas, accordingly. Images were converted to 8-bit grayscale, and the entire image was used as a region of interest. Collagen-stained area percentage (area %) was then measured.[31]

Immunohistochemical Staining of α-Smooth Muscle Actin (α-SMA)

Paraffin-embedded liver sections underwent deparaffinization using xylene, followed by rehydration in a descending ethanol series. Sections were immersed in citrate buffer (pH 6.0) and heated in a microwave system at 98°C for 20 minutes. After cooling in tap water for 10 minutes, the slides were incubated with 5% bovine serum albumin (5% BSA) for 60 minutes at room temperature to block nonspecific binding.

Subsequently, the slides were incubated in 3% hydrogen peroxide (H_2O_2) for 30 minutes to block endogenous peroxidase activity. Sections were then incubated with the primary anti-α-SMA antibody (1:1500 dilution) overnight at 4 °C, followed by incubation with horseradish peroxidase (HRP)-conjugated goat anti-rabbit IgG H&L secondary antibody (1:1000 dilution) for 30 minutes. Signal detection was performed using DAB working solution, and hematoxylin was used for counterstaining.[32]

Statistical Analysis

GraphPad Prism version 10.4 (GraphPad Software, Inc., La Jolla, CA) was used to analyze serological data, liver homogenate biomarkers, and fibrosis area quantification. All quantitative results are presented as mean ± standard deviation (SD). The Shapiro–Wilk test was applied to assess data normality. One-way analysis of variance (ANOVA) followed by the Tukey–Kramer post hoc test was used for group comparisons. A P-value of less than 0.05 ($P < 0.05$) was considered statistically significant.

Results

Characterization of AKBA-NLCs

Examination of AKBA-loaded nanostructured lipid carriers (AKBA-NLCs) via dynamic light scattering (DLS) revealed a primary size distribution centered between 202.4 nm and 226.8 nm across replicates with Z-average diameters ranging from 237.2 to 262.0 nm. The polydispersity index (PDI) values ranged from 0.392 to 0.484, indicating moderate polydispersity. Minor peaks corresponding to larger particle sizes (~5.5 µm) were observed at low intensity (0–1.1%), likely due to occasional aggregation.

The spherical morphology of the NLCs was confirmed by transmission electron microscopy (TEM) which showed particle diameters ranging from 107 to 133 nm. These findings confirm that the prepared NLCs fall within the nanoscale range and exhibit favorable morphology.

Zeta potential analysis indicated a mean surface charge of −4.82 mV with a standard deviation of 5.09 mV, based on 12 zeta runs. The instrument marked this result as "good," and the distribution curve exhibited a single, narrow peak, suggesting sample consistency Figure 1.

Serum Liver Function Tests

Liver function tests showed marked elevations in ALT and AST levels in Group 2 compared to Group 1 by 357.11% and

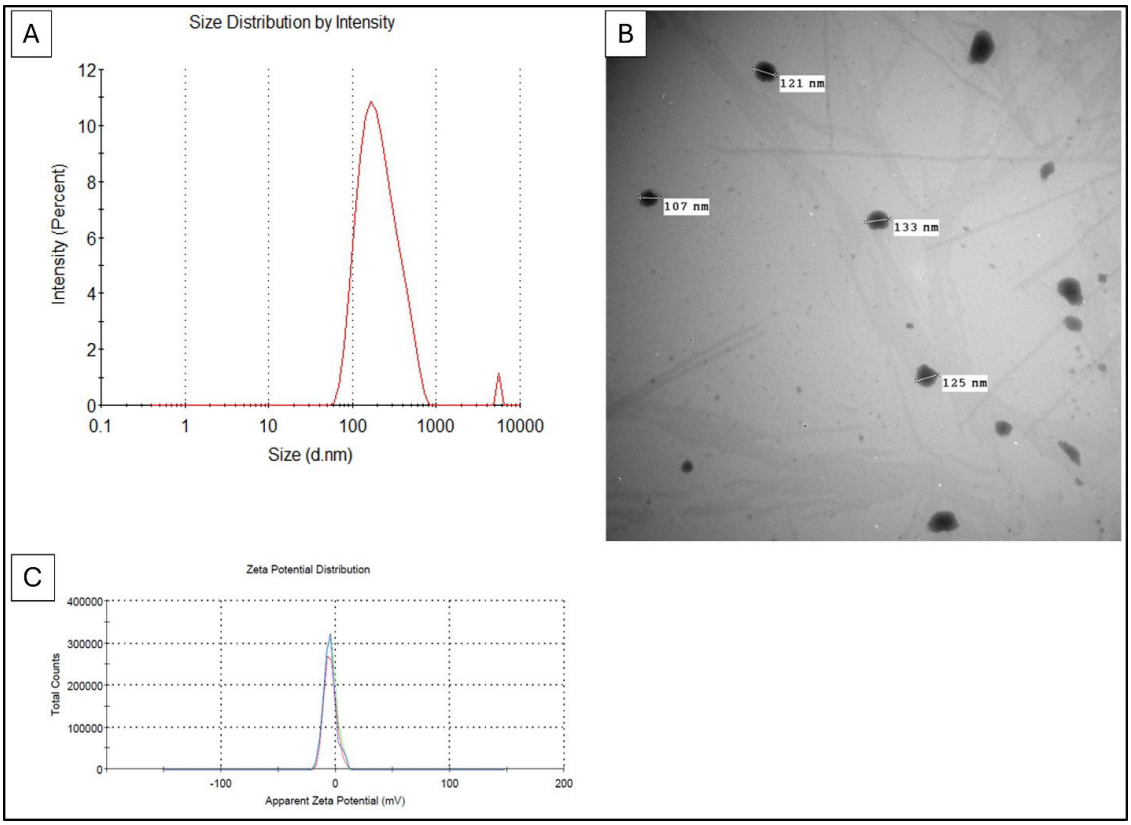

Fig. 1 **Characterization of AKBA-loaded nanostructured lipid carriers (AKBA-NLCs). (A) Dynamic light scattering (DLS) analysis showing the size distribution by intensity. The main peak corresponds to an average hydrodynamic diameter of 202–227 nm (226.8 ± 123.8 nm, PDI = 0.484), with a narrow distribution and minor signals attributed to aggregates. (B) Transmission electron microscopy (TEM) image displaying spherical nanoparticles with diameters ranging from 107 to 133 nm. (C) Zeta potential distribution indicating near-neutral surface charge (mean surface charge −4.82 mV ± 5.09 mV), suggesting low electrostatic stabilization.**

315.60% (P = 0.0002 and 0.0042), respectively, as shown in Figures 2A and 2B. Groups 3, 4, and 5 demonstrated significant reductions in ALT levels by 51.79%, 48.26%, and 73.13% (P = 0.0129, 0.03, and 0.0005), respectively. A significant reduction in AST was observed only in Group 5 by 72.90% (P = 0.0061), while Groups 3 and 4 showed no significant changes compared to Group 2, as illustrated in Figure 2B.

A significant reduction in serum albumin was noted in Group 2 by 58.8% (P = 0.0003) compared to Group 1. Treatment groups (Groups 3, 4, and 5) showed significant restoration of albumin levels by 109.12%, 160.09%, and 144.66% (P = 0.0046, 0.0001, and 0.0002), respectively, as shown in Figure 2C. Similarly, total bilirubin levels were markedly elevated in Group 2 by 151.45% (P < 0.0001), while Groups 3, 4, and 5 demonstrated significant reductions by 16.76%, 39.88%, and 66.89%, respectively (all P < 0.0001), as shown in Figure 2D.

Inflammatory Markers Assay

Liver homogenate analysis revealed a significant elevation in TNF-α levels in Group 2 by 245.8% (P < 0.0001) compared to Group 1. This elevation was significantly reduced in all treatment groups by 65.6% in Group 3, 64.8% in Group 4, and 62.3% in Group 5 (all P < 0.0001), as shown in Figure 3A.

Similarly, IL-1β levels increased by 156.7% in Group 2 compared to Group 1. Treatment significantly reduced IL-1β by 65.9% in Group 3, 55.0% in Group 4, and 58.3% in Group 5 (all P < 0.0001), as presented in Figure 3B.

IL-6 levels were also elevated by 145.2% in Group 2 versus Group 1. These were significantly attenuated by 63.9% in Group 3, 57.4% in Group 4, and 66.5% in Group 5 (all P < 0.0001), as shown in Figure 3C.

Reduced glutathione (GSH) levels decreased by 75.1% in Group 2 (P < 0.0001). Treatment significantly restored GSH levels by 334.1% in Group 3, 368.7% in Group 4, and 298.3% in Group 5 (all P < 0.0001), as shown in Figure 3D.

Lastly, liver homogenate malondialdehyde (MDA) levels were significantly elevated by 117.6% in Group 2 in relation to Group 1 (P = 0.0015). These elevations were significantly reduced by 82.2% in Group 3 (P = 0.0004), 75.4% in Group 4 (P = 0.7514), and 66.2% in Group 5 (P = 0.0024). MDA data are not shown for clarity and visual consistency.

Histopathology Results

Hematoxylin and Eosin (H&E) Examination

H&E-stained liver sections from Group 1 revealed preserved hepatic architecture, featuring classic hepatic lobules with a

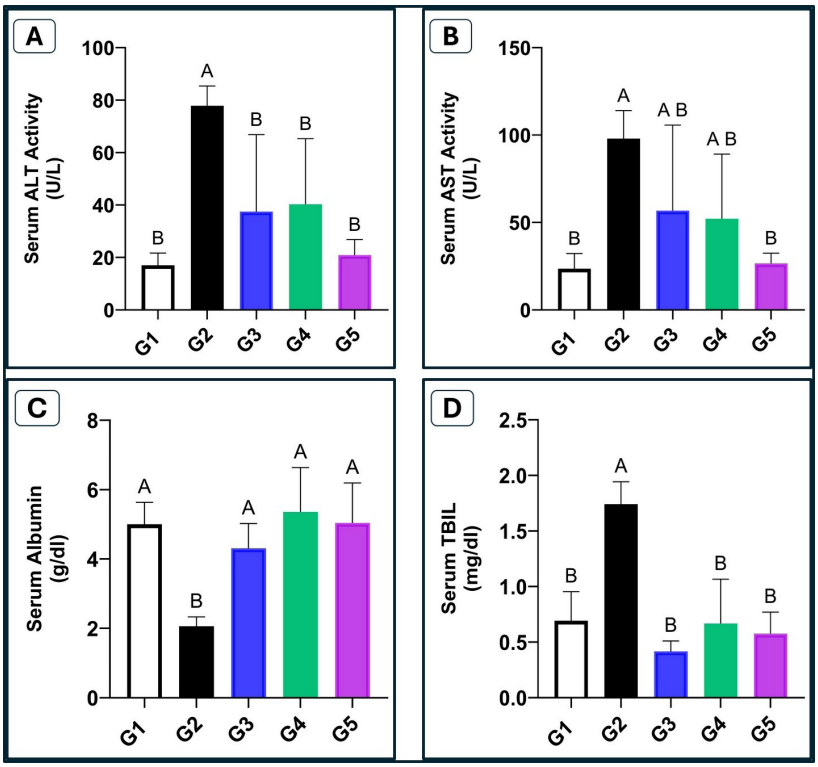

Fig. 2 **Effects of treatments on serum liver biomarkers across experimental groups. (A) Alanine aminotransferase (ALT), (B) aspartate aminotransferase (AST), (C) albumin, and (D) total bilirubin (TBIL) levels. Data are presented as mean ± SD ($n = 5$). Bars with different letters indicate statistically significant differences ($P < 0.05$) between groups based on one-way ANOVA followed by Tukey's post hoc test. Each treatment group was compared to both the negative control (Group 1) and the positive control (Group 2). G1: Normal control group; G2: TAA group; G3: TAA + MgO NPs group; G4: TAA + AKBA group; G5: TAA + AKBA-NLCs + MgO NPs group.**

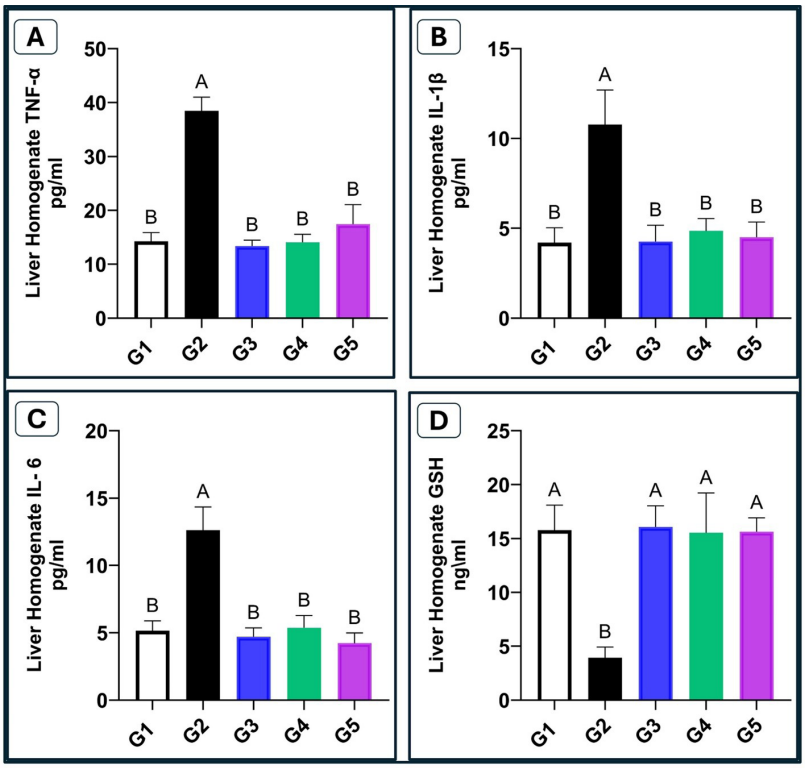

Fig. 3 **Effect of treatments on liver homogenate levels of inflammatory and antioxidant markers (A–D). (A) Tumor necrosis factor-α (TNF-α), (B) interleukin-1β (IL-1β), (C) interleukin-6 (IL-6), and (D) reduced glutathione (GSH). Data are presented as mean ± SD ($n = 5$). Bars with different letters indicate statistically significant differences ($P < 0.05$) between groups based on one-way ANOVA followed by Tukey's post hoc test. Each treatment group was compared to both the negative control (Group 1) and the positive control (Group 2). G1: Normal control group; G2: TAA model group; G3: TAA + MgO NPs group; G4: TAA + AKBA group; G5: TAA + AKBA-NLCs + MgO NPs group.**

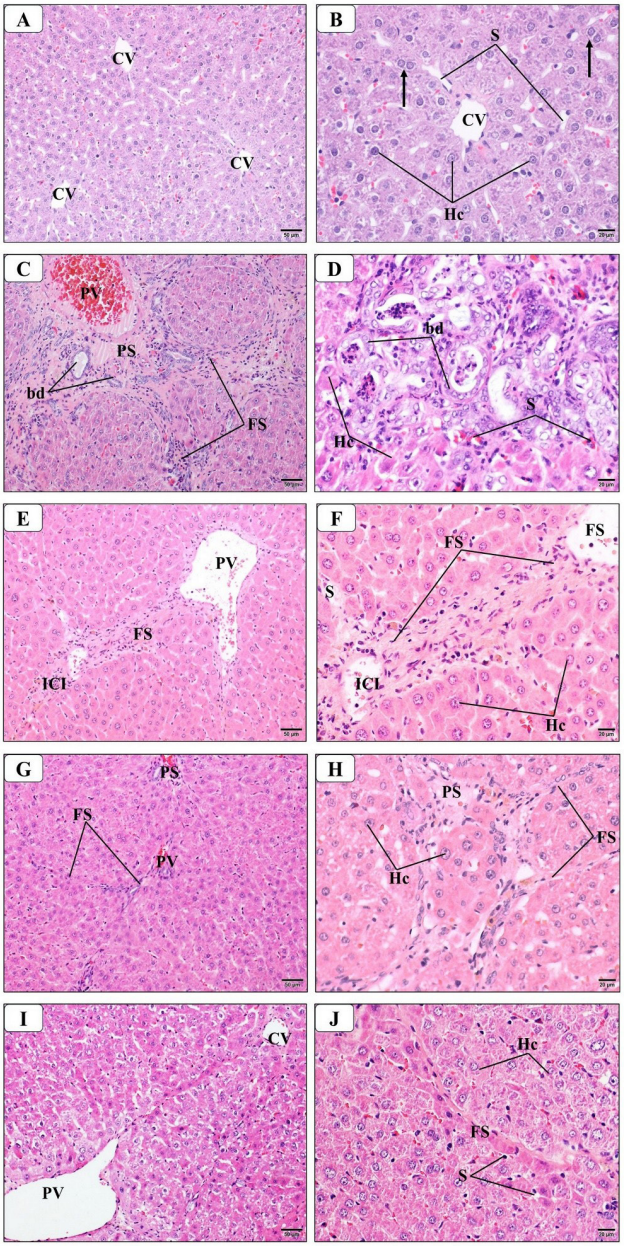

Fig. 4 **Representative H&E-stained liver sections from each experimental group. (A, B) Control group showing hepatic lobules with preserved architecture with hepatocyte cords (Hc) extending radially from the central vein (CV) toward the portal areas. Hepatocytes exhibit eosinophilic cytoplasm and contain one or two rounded nuclei (arrow). (C, D) TAA group showing that the normal hepatic lobule architecture is disrupted with pseudolobule (PS) and thickened fibrous septa (FS). Most hepatocytes (Hc) display nuclear condensation (pyknosis). (E, F) TAA + MgO NPs group showing improved lobular organization with minimal dilation of portal spaces (PS) and hepatocytes with near-normal morphology (Hc). Slight sinusoidal (S) dilation and focal inflammatory cell infiltration (ICI) are noted. PV = Portal Vein. (G, H) TAA + AKBA group showing mild architectural improvement with limited portal dilation and mostly preserved hepatocyte morphology (Hc). (I, J) TAA + AKBA-NLCs + MgO NPs group showing marked histological improvement, with restored lobular structure, regular hepatocyte cords (Hc), and minimal fibrosis or pseudolobule formation. (Magnification: Panels A, C, E, G, I at ×100; B, D, F, H, J at ×200).**

central vein, a radiating sinusoidal pattern, and a normal periportal structure. Hepatocytes exhibited vesicular nuclei with prominent nucleoli and granular cytoplasm, with occasional vacuolations, as shown in Figures 4A and 4B. Minimal inflammatory cell infiltration, likely lymphocytes, was observed in the portal areas. In contrast, Group 2 demonstrated significant architectural distortion, including pseudolobule formation, regenerative nodules, and bridging fibrosis between portal and central regions, as shown in Figures 4C and 4D.

Group 3 exhibited moderate histological improvement compared to Group 2. While mild portal and pericentral fibrosis with septations were present, no well-formed pseudolobules were observed. Moderate congestion of the portal veins was also noted, as shown in Figures 4E and 4F. Group 4 showed mild improvement relative to Group 2, although less pronounced than in Groups 3 and 5. Histological sections revealed diffuse portal bridging fibrosis and incomplete pseudolobule formation, as shown in Figures 4G and 4H. Occasional foci of micro-steatosis were also observed. Group 5 showed marked histological improvement compared to Group 2. Liver sections revealed preserved lobular architecture, absence of pseudolobule formation, and minimal portal fibrosis with little to no septation, as shown in Figures 4I and 4J.

Masson Trichrome Staining

Masson's Trichrome staining revealed minimal collagen existence around portal structures and preserved lobular structure in Group 1, as shown in Figure 5A. In contrast, there was extensive collagen deposition (blue-stained fibers) in Group 2. The fibrosis was staged as F3–F4 based on the METAVIR scoring system, consistent with advanced fibrosis, as shown in Figure 5B. Fibrosis area percent quantification using Image J software demonstrated a significant increase in collagen area percentage in Group 2 compared to Group 1 ($P < 0.0001$), as shown in Figure 5F. Although Groups 3 and 4 showed some reduction in collagen accumulation, as demonstrated in Figures 5C and 5D, Group 5 showed a significant reduction in collagen area percentage compared to Group 2 (all $P < 0.0001$). Group 3 had an estimated fibrosis score of F2–F3, while Group 4 scored F3. Group 5 showed significantly reduced collagen levels compared to both Group 3 ($P = 0.03$) and Group 4 ($P = 0.0001$), as shown in Figure 5F. All Masson's Trichrome-stained collagen quantifications are summarized in Figure 5F.

Immunohistochemical Results

Group 1 showed minimal expression of α-SMA only limited to portal structures and scarce around central vein, as shown in Figure 6A.

Group 2 showed diffuse heightened expression of α-SMA extending from central veins and delineating pseudolobules, as shown in Figure 6B. Group 3 showed moderate improvement suggested by the reduction in distribution and staining intensity around central veins, as shown in Figure 6C. Group 4 showed mild improvement as indicated by the excessive expression of α-SMA conforming to the pseudolobular pattern and excessive expansions from central veins resulting in bridging, as shown in Figure 6D. Group 5 showed a marked reduction in the expression of α-SMA, as indicated in Figure 6E. Group 5 showed the most significant suppression suggesting more effective inhibition of hepatic stellate cell activation by the combined regimen.

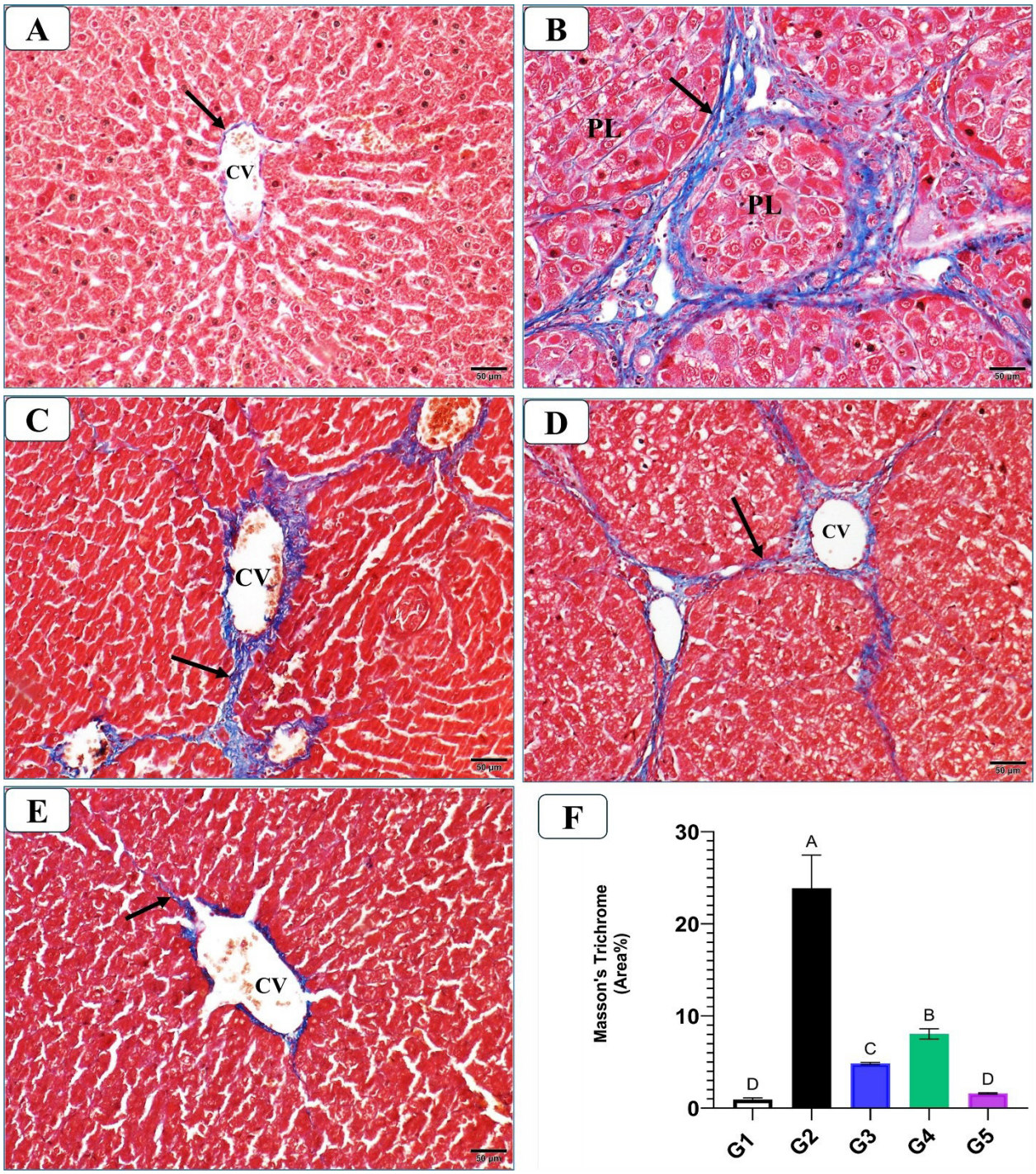

Fig. 5 **Representative photomicrographs of Masson's Trichrome-stained sections and quantitative analysis of collagen deposition in each group. (A) Control group showing normal hepatic architecture with minimal, blue-stained collagen fibers (arrow) around the central vein (CV). (B) TAA group displaying extensive collagen fibers (arrow) forming fibrotic septa enclosing pseudolobules (PL). (C) TAA + MgO NPs group showing moderate collagen fiber accumulation around the central vein (CV) and forming bridging septation (arrow). (D) TAA + AKBA group showing prominent collagen fiber septations (arrow) extending from the central vein (CV). (E) TAA + AKBA-NLCs + MgO NPs group showing near-normal collagen distribution with minimal perivenular collagen fiber extension (arrow). (F) Quantitative analysis of collagen area percentage measured from Masson's Trichrome-stained sections. Bars represent mean ± SD ($n = 5$). Bars labeled with different letters indicate statistically significant differences ($P < 0.05$) as determined by one-way ANOVA followed by Tukey's post hoc test. G1: Normal control group; G2: TAA group; G3: TAA + MgO NPs group; G4: TAA + AKBA group; G5: TAA + AKBA-NLCs + MgO NPs group. (Magnification: Panels A–E at ×100).**

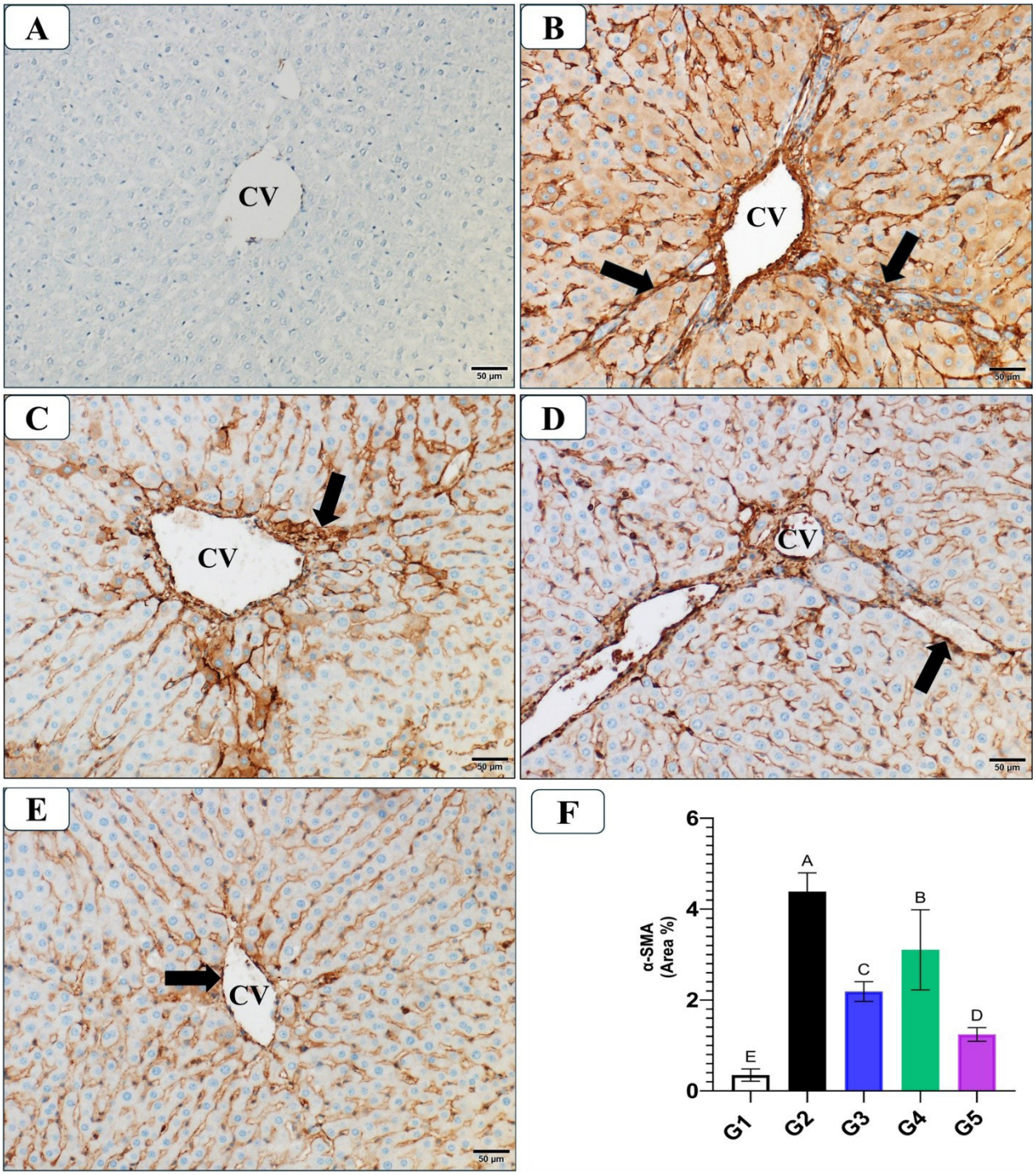

Fig. 6 **Representative α-Smooth Muscle Actin (α-SMA) expression around the central vein (CV) in each experimental group. (A) Normal control group showing absence of α-SMA expression around the central vein (CV). (B) TAA group showing strong α-SMA immunoreactivity in perisinusoidal areas and fibrous septa (arrows). (C) TAA + MgO NPs group showing a mild reduction in α-SMA expression around the central vein (CV) and within fibrous septations extending from the central vein (arrow). (D) TAA + AKBA group showing minimal reduction of α-SMA expression around the central vein (CV) and in the fibrous septation areas (arrow). (E) TAA + AKBA-NLCs + MgO NPs group showing minimal α-SMA immunostaining around central veins (CV) and no septations extending into the perivenular area (arrow). (F) Quantitative analysis of α-SMA–positive area percent (area %). Bars represent mean ± SD ($n = 5$). Bars labeled with different letters indicate statistically significant differences ($P < 0.05$) as determined by one-way ANOVA followed by Tukey's post hoc test. G1: Normal control group; G2: TAA group; G3: TAA + MgO NPs group; G4: TAA + AKBA group; G5: TAA + AKBA-NLCs + MgO NPs group. (Magnification: Panels A–E at ×100).**

Discussion

The observed discrepancy between particle sizes measured by dynamic light scattering (DLS) and transmission electron microscopy (TEM) is consistent with established findings for nanostructured lipid carriers (NLCs). DLS analysis yielded hydrodynamic diameters in the range of 202–227 nm, while TEM images revealed physical particle sizes between 107 and 133 nm. This variation is expected due to the different principles underlying each technique. DLS measures the hydrodynamic diameter, which includes the nanoparticle core along with the solvation layer and any surface-bound lipids or stabilizers, often resulting in larger apparent sizes.[33,34] In contrast, TEM provides direct visualization of dehydrated particles in a vacuum, reflecting only the solid core structure. As reported by Bhattacharjee et al., if TEM shows particles around 100 nm, DLS may report sizes as large as 120–160 nm or even up to 200 nm, depending on hydration layers and polydispersity.[35] Although the magnitude of the zeta potential was relatively low, the near-neutral surface charge is characteristic of lipid-based carriers stabilized by nonionic surfactants, where steric hindrance contributes more significantly to colloidal stability than electrostatic repulsion.

The 50–80% increase in size observed by DLS relative to TEM falls within the acceptable range for lipid-based nanocarriers, especially considering the moderate polydispersity (PDI: 0.392–0.484) observed in the formulation. Additionally, the presence of minor peaks corresponding to larger sizes in the DLS profile likely reflects low-abundance aggregates, which are often undetectable in TEM due to sample preparation limitations or a restricted field of view. These combined results confirm the successful formation of nanosized particles with favorable morphology and colloidal stability for drug delivery applications.

Chronic liver disease is a significant global health problem with a substantial burden.[1] It often progresses to liver fibrosis and, eventually, cirrhosis.[25] The definitive treatment for liver cirrhosis is liver transplantation.[36] The hallmark of liver fibrosis is the excessive accumulation of extracellular matrix proteins, which disrupts the normal liver architecture in response to chronic injury.[3]

There are no animal liver fibrosis models that mimic human liver fibrosis exactly.[37] To study liver fibrosis, well-established animal models have been developed, including carbon tetrachloride, dimethyl nitrosamine, diethyl nitrosamine, and thioacetamide (TAA), along with others like bile duct ligation.[38] Predominant regenerative nodules are more conspicuous in the TAA model when compared to the carbon tetrachloride model.[39] Also, the TAA rodent model is known for its long-lasting fibrotic changes for 2 months after cessation of the offending agent.[37] Furthermore, the TAA animal model shows lower mortality when compared to the carbon tetrachloride model.[8] Although the exact mechanisms are poorly understood, the TAA model of liver fibrosis is closely related to alcoholic fibrogenesis observed in humans.[8] TAA is known for inducing oxidative stress and centrilobular necrosis, portal-portal and portal-central bridging fibrosis, bile ductules proliferation, and portal inflammatory cell infiltration, consistent with our findings in the TAA group (Group 2). All the observed pathological features in our TAA group of Wistar rats in this study are in line with the findings in the literature.

In the current study, all our treatment groups showed varying degrees of improvement in the stage of liver fibrosis. MgO NPs are a recent trend in material science and biology. However, the literature lacks studies testing MgO NPs as a potential treatment, and they have not been extensively implemented in liver research. Additionally, MgO NPs can indirectly reduce oxidative stress by promoting endogenous antioxidant systems. In a study by Mittag *et al.*, MgO NPs were evaluated for cytotoxicity in HT29 human intestinal cells. Using transmission electron microscopy (TEM), no morphological changes were observed at concentrations up to 100 µg/mL. Furthermore, assessments including the 3-(4,5-dimethylthiazol-2-yl)-2,5-diphenyltetrazolium bromide assay (MTT) assay, 4',6-diamidino-2-phenylindole (DAPI) staining, and formamidopyrimidine-DNA glycosylase (FPG) assay revealed no significant differences in metabolic activity or DNA damage compared to control cells.[40] These findings suggest that MgO NPs exhibit minimal cytotoxicity in intestinal epithelial cells, indicating their potential safety and applicability in therapeutic contexts such as liver fibrosis. In a study conducted by Mazaheri *et al.*, liver histological analysis showed sinusoidal congestion in various non-specific regions and proliferation of bile ductules.[26] Majeed *et al.* tested MgO NPs at various dosages of 62.5, 125, 250, and 500 mg/kg/day, administered orally for 28 days, to study their toxicity.[41] Majeed and colleagues found that liver accumulation has occurred at 500 mg/kg/day but not in other doses. Interestingly, no kidney accumulation occurred at all doses. White blood cell count, hemoglobin concentration, and lymphocyte count were elevated in comparison to the control group starting at 62.5 mg/kg/day.[41] These elevations of blood indices were observed at much lower concentrations of 250 and 500 µg/ml/day every other day for 28 days, as documented by Mazaheri *et al.*[26] Moreover, aspartate aminotransferase (AST) increased significantly at a dose of 125 µg/ml/day.[26] Therefore, we used a very minimal volume-based dose of MgO NPs based on the effects documented by these previous studies. We observed mild central vein congestion in the MgO NPs-treated group at a lower concentration of 100 µg/ml/day in our study. These converging data underpin the view that MgO-NPs can be utilized as safe antioxidant-enhancing agents in settings such as liver fibrosis, where oxidative stress drives disease progression.

AKBA is a pentacyclic triterpenoid derived from Boswellia serrata and is known for its potent anti-inflammatory and antioxidant properties. At the molecular level, AKBA has been shown to inhibit the nuclear factor-kappa B (NF-κB) pathway, a key transcription factor involved in the regulation of pro-inflammatory cytokines such as TNF-α, IL-1β, and IL-6.[10,42] AKBA blocks inhibitor of kappa B (IκB) kinase activity, thereby preventing the phosphorylation and subsequent degradation of inhibitor of kappa B alpha (IκBα), which sequesters NF-κB in the cytoplasm.[43] This inhibition downregulates the transcription of inflammatory mediators and attenuates immune cell infiltration in injured hepatic tissues. In addition to NF-κB, AKBA also modulates the nuclear factor erythroid 2–related factor 2 / antioxidant response element (Nrf2/ARE) signaling pathway. Activation of Nrf2 leads to transcription of antioxidant enzymes such as heme oxygenase-1 (HO-1), glutathione peroxidase (GPx), and superoxide dismutase

(SOD), which collectively reduce oxidative stress and lipid peroxidation.[10]

Kachoiu *et al*. tested the effects of AKBA as a preventive and therapeutic agent in a high-fructose diet model of non-alcoholic fatty liver disease (NAFLD) in rats. The prevention group received AKBA and a high-fructose diet concurrently for six weeks, while the treatment group received a four-week high-fructose diet followed by a two-week AKBA treatment. Moreover, AKBA significantly decreased, and nearly normalized, serum ALT and AST levels in both groups. Furthermore, the inflammatory cytokines TNF-α and IL-6 were significantly reduced by AKBA. However, AKBA reduced the level of transforming growth factor beta (TGF-β) only in the treatment group, not in the prevention group.[11] This may explain our findings that AKBA improved serological and liver homogenate biomarkers, though it had no significant effect on collagen deposition or α-SMA immunohistochemical expression. This outcome could be due to the concurrent administration of TAA with AKBA, causing a persistent induction of TGF-β and subsequent α-SMA activation.

Previous AKBA formulations, such as PLGA nanoparticles, have improved the systemic exposure of AKBA; however, nanostructured lipid carriers (NLCs) offer additional advantages in encapsulating lipophilic agents, enhancing bioavailability, and promoting lymphatic uptake.[22] In this study, AKBA was incorporated into an NLC formulation to improve its therapeutic efficacy in TAA-induced liver fibrosis.

The combination of AKBA-NLCs and MgO NPs is a novel approach designed to enhance the antioxidant capabilities of MgO NPs and the anti-inflammatory potential of AKBA, while improving its oral bioavailability through encapsulation in nanostructured lipid carriers. While research on MgO NPs and NLCs is still emerging, our findings contribute to the growing understanding of their combined effects on liver fibrosis. The AKBA-NLCs + MgO NPs-treated group (Group 5) showed substantial improvement in pseudolobule distribution, collagen fiber deposition, and cell viability. On histological quantitative assessment, it showed a significant improvement in collagen content and inhibition of α-SMA activation in comparison to the AKBA-treated group (Group 4) and the MgO NPs-treated group (Group 3).

Although AKBA is inherently hydrophobic and poorly water-soluble, the development of nanostructured lipid carriers (NLCs) allowed for its dispersion into a stable colloidal form. While this approach may not alter intrinsic aqueous solubility, it facilitates enhanced gastrointestinal absorption—potentially through intestinal M cells and lymphatic transport—and thereby improves its oral bioavailability.[24]

We acknowledge that many anti-fibrotic therapies that show promise in preclinical liver fibrosis models have struggled to translate to clinical practice due to challenges such as manufacturing complexity, safety uncertainties, and the need for long-term efficacy.[44] Our AKBA-NLCs and MgO NPs combination was specifically designed with biocompatibility and biodegradability in mind. MgO NPs gradually dissolve into magnesium ions, which are naturally metabolized or excreted, distinguishing them from heavy metal nanoparticles such as silver or cadmium that can leave toxic residues.[45,46] Additionally, our nanostructured lipid carriers (NLCs) system is formulated using GRAS-classified lipids that are non-toxic, non-immunogenic, and enzymatically biodegradable.[46] Recent studies further support the excellent in vivo biocompatibility and low immunogenicity of such lipid-based carriers.[46] These materials collectively enhance the safety and tolerability of our formulation, supporting its suitability for clinical translation.

We also address key challenges related to scalability and regulatory approval. Transitioning from lab-scale synthesis to industrial-scale manufacturing requires consistent control over nanoparticle size, charge, and surface properties to ensure therapeutic uniformity. Notably, NLC-based formulations are known for their scalability and cost-effective production. Our approach also avoids the use of toxic organic solvents, supporting environmentally sustainable manufacturing practices.[47] Regarding regulation, nanotherapies must meet rigorous pharmacokinetic, toxicologic, and quality control benchmarks. The success of nanomedicines like liposomal doxorubicin (Doxil®) has paved the way for broader clinical acceptance.[48] Building on our encouraging efficacy results, we propose advancing formal pharmacokinetic and dose-finding studies, which are essential for defining safe and effective clinical protocols. Literature supports that once these translational challenges are addressed, nanomedicine-based antifibrotic strategies are likely to become viable treatment options.[49] Liver fibrosis is a progressive and often relapsing condition, and long-term therapeutic efficacy is essential for clinical translation. Although our study demonstrated significant histological and biochemical improvements within a 4-week treatment window, it remains unclear whether these antifibrotic effects would be sustained following treatment cessation or during extended therapy. Therefore, we have now included in the discussion that future studies with longer treatment durations (e.g., 8–12 weeks or more), along with post-treatment follow-up phases, are necessary to assess the durability of therapeutic response and the potential for fibrosis rebound or progression. This approach aligns with previous preclinical research emphasizing the need for prolonged observation to confirm sustained collagen resolution and reversal of fibrogenic signaling.[50] Additionally, we acknowledge the importance of evaluating the long-term safety of magnesium oxide nanoparticles (MgO NPs). While magnesium is a physiologically essential mineral, its nanoparticulate form may exhibit altered biodistribution and toxicity depending on dose, surface properties, and administration route. In our study, no acute toxicity or behavioral abnormalities were observed in the MgO NPs-treated rats. Nonetheless, potential risks such as nanoparticle accumulation, dose-dependent toxicity, and immune system interactions must be carefully considered, particularly with chronic or high-dose exposure.

In conclusion, liver fibrosis is a multifactorial disease with diverse etiologies; yet many forms share common pathological mechanisms such as oxidative stress and inflammation. In this study, we targeted these processes by combining the antioxidant properties of magnesium oxide nanoparticles (MgO NPs) with the anti-inflammatory effects of Acetyl-11-Keto-β-Boswellic Acid (AKBA). To enhance the efficacy and bioavailability of AKBA, we formulated it using nanostructured lipid carriers (AKBA-NLCs). This combination of AKBA-NLCs and MgO NPs demonstrated promising therapeutic effects in a preclinical rat model of liver fibrosis, with improvements observed both histologically and serologically.

Limitations

This study has certain limitations due to logistical constraints, including the absence of funding and time. The small number of rats per group (n = 5), the lack of long-term follow-up on research endpoints, and the absence of detailed drug toxicity assessments are notable limitations. We encourage further exploration on a larger scale with extended treatment duration and comprehensive safety evaluation.

Author Contributions

Afraa Alsamkari: conceptualization, methodology, investigation, formal analysis, data curation, visualization, writing – original draft, writing – review & editing, Funding acquisition. The other co-authors contributed to supervision and manuscript review. All authors have read and agreed to the published version of the manuscript.

Acknowledgments

We would like to express our sincere appreciation to Prof. Osama Abdelhakim Aly Ahmed for his invaluable guidance in nanotechnology formulation and supervision throughout this study. I am also grateful to Mr. Thamer Shaker from King Fahad Medical Research Center for his technical assistance with the animal experiments.

Declaration of Conflicting Interests

The author(s) declared no potential conflicts of interest with respect to the research, authorship, and/or publication of this article.

Funding

This research did not receive any specific grant from funding agencies in the public, commercial, or not-for-profit sectors.

References

1. Nalkurthi C, Schroder WA, Melino M, Irvine KM, Nyuydzefe M, Chen W, et al. ROCK2 inhibition attenuates profibrogenic immune cell function to reverse thioacetamide-induced liver fibrosis. JHEP Rep. 2022;4(1):100386. Available from: https://www.sciencedirect.com/science/article/pii/S2589555921001622
2. Jangra A, Kothari A, Sarma P, Medhi B, Omar BJ, Kaushal K. Recent advancements in antifibrotic therapies for regression of liver fibrosis. Cells. 2022;11(9):1500. Available from: https://www.mdpi.com/2073-4409/11/9/1500
3. Berumen J, Baglieri J, Kisseleva T, Mekeel K. Liver fibrosis: pathophysiology and clinical implications. WIREs Mech Dis. 2021;13(1):e1499. Available from: https://wires.onlinelibrary.wiley.com/doi/full/10.1002/wsbm.1499
4. Kim HY, Sakane S, Eguileor A, Carvalho Gontijo Weber R, Lee W, Liu X, et al. The origin and fate of liver myofibroblasts. Cell Mol Gastroenterol Hepatol. 2024;17(1):93–106. Available from: https://www.sciencedirect.com/science/article/pii/S2352345X23001704
5. Gan L, Jiang Q, Huang D, Wu X, Zhu X, Wang L, et al. A natural small molecule alleviates liver fibrosis by targeting apolipoprotein L2. Nat Chem Biol. 2025;21(1):80–90. Available from: https://www.nature.com/articles/s41589-024-01704–3
6. Chen L, Guo W, Mao C, Shen J, Wan M. Liver fibrosis: pathological features, clinical treatment and application of therapeutic nanoagents. J Mater Chem B. 2024;12(6):1446–66. Available from: https://pubs.rsc.org/en/content/articlelanding/2023/tb/d3tb02790b
7. Moeini-Nodeh S, Rahimifard M, Baeeri M, Abdollahi M. Functional improvement in rats' pancreatic islets using magnesium oxide nanoparticles through antiapoptotic and antioxidant pathways. Biol Trace Elem Res. 2017;175(1):146–55. Available from: https://link.springer.com/article/10.1007/s12011-016-0754-8
8. Wallace M, Hamesch K, Lunova M, Kim Y, Weiskirchen R, Strnad P, et al. Standard operating procedures in experimental liver research: thioacetamide model in mice and rats. Lab Anim. 2015;49(1 Suppl):21–9. Available from: https://journals.sagepub.com/doi/full/10.1177/0023677215573040
9. Nisa FY, Rahman MA, Rafi MKJ, Khan MAN, Sultana F, Majid M, et al. Biosynthesized magnesium oxide nanoparticles from Tamarindus indica seed attenuate doxorubicin-induced cardiotoxicity by regulating biochemical indexes and linked genes. Biomater Adv. 2023;146:213291. Available from: https://www.sciencedirect.com/science/article/abs/pii/S2772950823000146
10. Roy NK, Parama D, Banik K, Bordoloi D, Devi AK, Thakur KK, et al. An update on pharmacological potential of boswellic acids against chronic diseases. Int J Mol Sci. 2019;20(17):4101. Available from: https://www.mdpi.com/1422-0067/20/17/4101
11. Kachouei RA, Doagoo A, Jalilzadeh M, Khatami SH, Rajaei S, Jahan-Abad AJ, et al. Acetyl-11-keto-beta-boswellic acid has therapeutic benefits for NAFLD rat models that were given a high fructose diet by ameliorating hepatic inflammation and lipid metabolism. Inflammation. 2023;46(5):1966–80. Available from: https://link.springer.com/article/10.1007/s10753-023-01853-y
12. Pu S, Li Y, Liu Q, Zhang X, Chen L, Li R, et al. Inhibition of 5-lipoxygenase in hepatic stellate cells alleviates liver fibrosis. Front Pharmacol. 2021;12:628583. Available from: https://www.frontiersin.org/journals/pharmacology/articles/10.3389/fphar.2021.628583/full
13. Siddiqui MZ. Boswellia serrata, a potential antiinflammatory agent: an overview. Indian J Pharm Sci. 2011;73(3):255–61. Available from: https://www.ncbi.nlm.nih.gov/pmc/articles/PMC3309643/
14. Krüger P, Kanzer J, Hummel J, Fricker G, Schubert-Zsilavecz M, Abdel-Tawab M. Permeation of Boswellia extract in the Caco-2 model and possible interactions of its constituents KBA and AKBA with OATP1B3 and MRP2. Eur J Pharm Sci. 2009;36(2):275–84. Available from: https://www.sciencedirect.com/science/article/abs/pii/S0928098708004272
15. Ale-Ahmad A, Kazemi S, Daraei A, Sepidarkish M, Moghadamnia AA, Parsian H. pH-sensitive nanoformulation of Acetyl-11-Keto-beta-Boswellic Acid (AKBA) as a potential antiproliferative agent in colon carcinogenesis (in vitro and in vivo). BMC Complement Med Ther. 2024;24:289. Available from: https://link.springer.com/article/10.1186/s12645-024-00289-9
16. Bairwa K, Jachak SM. Development and optimisation of 3-Acetyl-11-keto-β-boswellic acid loaded poly-lactic-co-glycolic acid-nanoparticles with enhanced oral bioavailability and in-vivo anti-inflammatory activity in rats. J Pharm Pharmacol. 2015;67(9):1188–97. Available from: https://academic.oup.com/jpp/article-abstract/67/9/1188/6128233
17. Goel A, Ahmad FJ, Singh RM, Singh GN. 3-Acetyl-11-keto-β-boswellic acid loaded-polymeric nanomicelles for topical anti-inflammatory and anti-arthritic activity. J Pharm Pharmacol. 2010;62(2):273–8. Available from: https://academic.oup.com/jpp/article-abstract/62/2/273/6135770
18. Khan A, Al-Harrasi A, Rehman NU, Sarwar R, Ahmad T, Ghaffar R, et al. Loading AKBA on surface of silver nanoparticles to improve their sedative-hypnotic and anti-inflammatory efficacies. Nanomedicine. 2019;14(21):2783–98. Available from: https://www.tandfonline.com/doi/abs/10.2217/nnm-2019-0211
19. Su X, Zhong H, Zeng Y, Zhang Y, Zhang B, Guo W, et al. Dual-ligand-functionalized nanostructured lipid carriers as a novel dehydrocavidine delivery system for liver fibrosis therapy. Colloids Surf B Biointerfaces. 2025;246:114376. Available from: https://www.sciencedirect.com/science/article/abs/pii/S0927776524006350?via%3Dihub
20. Goel R, Mishra R, Singh N, Rajora A, Singh R, Gaur PK. Nanostructured lipid carriers: enhancing herbal medicine delivery. In: Lipid Based Nanocarriers for Drug Delivery. 2024. p. 367. Available from: https://www.researchgate.net/profile/Neelam-Singh-38/publication/382306507_'Nanostructured_Lipid_Carriers_Enhancing_Herbal_Medicine_Delivery'/links/66cb21b7c2eaa5002315fbf2/Nanostructured-Lipid-Carriers-Enhancing-Herbal-Medicine-Delivery.pdf#page=375

21. Bartneck M, Warzecha KT, Tacke F. Therapeutic targeting of liver inflammation and fibrosis by nanomedicine. Hepatobiliary Surg Nutr. 2014;3(6):364–76. Available from: https://pmc.ncbi.nlm.nih.gov/articles/PMC4273112/
22. Desai PP, Date AA, Patravale VB. Overcoming poor oral bioavailability using nanoparticle formulations–opportunities and limitations. Drug Discov Today Technol. 2012;9(2):e87–95. Available from: https://www.sciencedirect.com/science/article/abs/pii/S1740674911000345
23. He C, Yin L, Tang C, Yin C. Multifunctional polymeric nanoparticles for oral delivery of TNF-α siRNA to macrophages. Biomaterials. 2013;34(11):2843–54. Available from: https://www.sciencedirect.com/science/article/abs/pii/S0142961213000495
24. Ajiboye AL, Nandi U, Galli M, Trivedi V. Olanzapine loaded nanostructured lipid carriers via high shear homogenization and ultrasonication. Sci Pharm. 2021;89(2):25. Available from: https://www.mdpi.com/2218-0532/89/2/25
25. Alkreathy HM, Esmat A. Lycorine ameliorates thioacetamide-induced hepatic fibrosis in rats: Emphasis on antioxidant, anti-inflammatory, and STAT3 inhibition effects. Pharmaceuticals. 2022;15(3):369. Available from: https://www.mdpi.com/1424-8247/15/3/369
26. Mazaheri N, Naghsh N, Karimi A, Salavati H. In vivo toxicity investigation of magnesium oxide nanoparticles in rat for environmental and biomedical applications. Iran J Biotechnol. 2019;17(1):e1543. Available from: https://pmc.ncbi.nlm.nih.gov/articles/PMC6697860/
27. Sharawy MH, El-Awady MS, Makled MN. Protective effects of paclitaxel on thioacetamide-induced liver fibrosis in a rat model. J Biochem Mol Toxicol. 2021;35(5):e22745. Available from: https://onlinelibrary.wiley.com/doi/full/10.1002/jbt.22745
28. ElBaset MA, Salem RS, Ayman F, Ayman N, Shaban N, Afifi SM, et al. Effect of empagliflozin on thioacetamide-induced liver injury in rats: role of AMPK/SIRT-1/HIF-1α pathway in halting liver fibrosis. Antioxidants. 2022;11(11):2152. Available from: https://www.mdpi.com/2076-3921/11/11/2152
29. Suvarna KS, Layton C, Bancroft JD. Bancroft's Theory and Practice of Histological Techniques. 8th ed. London: Elsevier Health Sciences; 2018.
30. Mohamadnejad M, Tavangar SM, Sotoudeh M, Kosari F, Khosravi M, Geramizadeh B, et al. Histopathological study of chronic hepatitis B: a comparative study of Ishak and METAVIR scoring systems. Int J Organ Transplant Med. 2010;1(4):171–6. Available from: https://pmc.ncbi.nlm.nih.gov/articles/PMC4089240/
31. Alavifard H, Mazhari S, Meyfour A, Tokhanbigli S, Ghavami S, Zali MR, et al. Imatinib suppresses activation of hepatic stellate cells by targeting STAT3/IL-6 pathway through miR-124. Cell Biol Int. 2023;47(5):969–80. Available from: https://onlinelibrary.wiley.com/doi/full/10.1002/cbin.11992
32. Ye J, Chen J, Li Y, Sun L, Lu H. Hepatocyte-specific knockout of HIF-2α cannot alleviate carbon tetrachloride-induced liver fibrosis in mice. PeerJ. 2023;11:e15191. Available from: https://peerj.com/articles/15191/
33. Danaei M, Dehghankhold M, Ataei S, Hasanzadeh Davarani F, Javanmard R, Dokhani A, et al. Impact of particle size and polydispersity index on the clinical applications of lipidic nanocarrier systems. Pharmaceutics. 2018;10(2):57. Available from: https://www.mdpi.com/1999-4923/10/2/57
34. Domingos RF, Tufenkji N, Wilkinson KJ. Aggregation of titanium dioxide nanoparticles: role of a fulvic acid. Environ Sci Technol. 2009;43(5):1282–6. Available from: https://pubs.acs.org/doi/abs/10.1021/es8023594
35. Bhattacharjee S. DLS and zeta potential–what they are and what they are not? J Control Release. 2016;235:337–51. Available from: https://www.sciencedirect.com/science/article/abs/pii/S0168365916303832
36. Terrault NA, Francoz C, Berenguer M, Charlton M, Heimbach J. Liver transplantation 2023: status report, current and future challenges. Clin Gastroenterol Hepatol. 2023;21(8):2150–66. Available from: https://www.sciencedirect.com/science/article/pii/S1542356523002781
37. Enciso N, Amiel J, Fabián-Domínguez F, Pando J, Rojas N, Cisneros-Huamaní C, et al. Model of liver fibrosis induction by thioacetamide in rats for regenerative therapy studies. Anal Cell Pathol (Amst). 2022;2022:2841894. Available from: https://onlinelibrary.wiley.com/doi/full/10.1155/2022/2841894
38. Bao YL, Wang L, Pan HT, Zhang TR, Chen YH, Xu SJ, et al. Animal and organoid models of liver fibrosis. Front Physiol. 2021;12:666138. Available from: https://www.frontiersin.org/journals/physiology/articles/10.3389/fphys.2021.666138/full
39. Norasingha A, Pradidarcheep W, Chayaburakul K. Chronological production of thioacetamide-induced cirrhosis in the rat with no mortality. J Med Assoc Thai. 2012;95(Suppl 7):S173–7. Available from: https://europepmc.org/article/med/23964462
40. Mittag A, Schneider T, Westermann M, Glei M. Toxicological assessment of magnesium oxide nanoparticles in HT29 intestinal cells. Arch Toxicol. 2019;93(6):1491–1500. Available from: https://link.springer.com/article/10.1007/s00204-019-02451-
41. Majeed SI, Mohammed SM, Mohammad AM. Bioaccumulation and evaluation of magnesium oxide nanoparticles toxicity and combination effects of vitamin E and C with it on exposed male rats. Kurdistan J Appl Res. 2023:1–10. Available from: https://mail.spu.edu.iq/kjar/index.php/kjar/article/view/813
42. Ammon H. Modulation of the immune system by Boswellia serrata extracts and boswellic acids. Phytomedicine. 2010;17(11):862–7. Available from: https://www.sciencedirect.com/science/article/abs/pii/S0944711310000620
43. Takada Y, Ichikawa H, Badmaev V, Aggarwal BB. Acetyl-11-keto-β-boswellic acid potentiates apoptosis, inhibits invasion, and abolishes osteoclastogenesis by suppressing NF-κB and NF-κB-regulated gene expression. J Immunol. 2006;176(5):3127–40. Available from: https://journals.aai.org/jimmunol/article/176/5/3127/73226
44. Addissouky TA, Ali MM, El Sayed IET, Wang Y, El Baz A, Elarabany N, et al. Preclinical promise and clinical challenges for innovative therapies targeting liver fibrogenesis. Arch Gastroenterol Res. 2023;4(1):14–23. Available from: https://www.scientificarchives.com/abstract/preclinical-promise-and-clinical-challenges-for-innovative-therapies-targeting-liver-fibrogenesis
45. Saberi A, Baltatu MS, Vizureanu P. Recent advances in magnesium–magnesium oxide nanoparticle composites for biomedical applications. Bioengineering. 2024;11(5):508. Available from: https://www.mdpi.com/2306-5354/11/5/508
46. Stefanova D, Yordanov Y, Bogdanova R, Voycheva C, Tzankov B, Popova T, et al. In vitro evaluation of the safety and antineoplastic effects in gastrointestinal tumors of nanostructured lipid carriers loaded with berberine. Pharmaceutics. 2025;17(3):331. Available from: https://www.mdpi.com/1999-4923/17/3/331
47. Duong VA, Nguyen TTL, Maeng HJ. Preparation of solid lipid nanoparticles and nanostructured lipid carriers for drug delivery and the effects of preparation parameters of solvent injection method. Molecules. 2020;25(20):4781. Available from: https://www.mdpi.com/1420-3049/25/20/4781
48. Ahmad S, Idris RAM, Wan Hanaffi WN, Perumal K, Boer JC, Plebanski M, et al. Cancer nanomedicine and immune system—interactions and challenges. Front Nanotechnol. 2021;3:681305. Available from: https://www.frontiersin.org/articles/10.3389/fnano.2021.681305/full
49. Gu L, Zhang F, Wu J, Zhuge Y. Nanotechnology in drug delivery for liver fibrosis. Front Mol Biosci. 2022;8:804396. Available from: https://www.frontiersin.org/journals/molecular-biosciences/articles/10.3389/fmolb.2021.804396/full
50. Kisseleva T, Brenner D. Molecular and cellular mechanisms of liver fibrosis and its regression. Nat Rev Gastroenterol Hepatol. 2021;18(3):151–66. Available from: https://www.nature.com/articles/s41575-020-00372-7